Progress In Electromagnetics Research C, Vol. 117, 115–127, 2021

A Crescent-Shaped Monopole MIMO Antennas with Improved Isolation for Dual-Band WLAN Applications

Likaa S. Yahya[1], Loay S. Yahya[1], and Khalil H. Sayidmarie[2, *]

Abstract—A multi-input multi-output (MIMO) antenna system is presented for wireless devices operating at WLAN (2.45, 5.25, and 5.775 GHz) bands. Each of the two antennas in the MIMO system consists of a crescent-shaped monopole whose first part covers the 2.45 GHz band while its second part covers the 5.25 GHz and 5.775 GHz bands. The second part of the monopole is a slot etched in the protruded ground plane between the two antennas. A decoupling mechanism in the form of two interlaced ring-shaped slots is used. The proposed MIMO antenna system is designed on an FR4 substrate with overall dimensions of $40 \times 47.5 \times 1.5$ mm and a small edge-to-edge spacing of 7.3 mm between two antennas. According to the measured results, the proposed design covers two frequency bands (2.2–2.83 GHz and 5.03–5.95 GHz) and has a mutual coupling of -20.78 dB at 2.45 GHz and -42.65 dB at 5.55 GHz. The proposed antenna's performance in both simulations and testing indicates that it is a good choice for WLAN applications.

1. INTRODUCTION

With the increasing demand for MIMO systems for various wireless communication applications, there is a need for placing more than one antenna in a limited space. When two or more antennas are located in near proximity, mutual coupling arises between them. This can result in the degradation of their radiation patterns and impedance matching. Various techniques to reduce the mutual coupling as well as increase the compactness of antenna elements in MIMO systems have been presented [1]. The used schemes to increase the isolation include electromagnetic bandgap EBG structure placed between two antennas [2], meander line structure [3–5], and various types of slots impeded between MIMO elements [6–12]. The self-curing decoupling technique has been used to reduce the mutual coupling by inlaying lumped element capacitors on the ground plane [13]. Neutralization of the leaked signal was proposed to reduce the mutual coupling where a suspended line interconnecting the two elements can supply the canceling signal [14–16]. Defective ground structures (DGS) were also used to reduce the signal coupled through the ground plane [1, 17]. Isolation can be improved by using decoupling networks [18, 19]. The specific orientation of the antenna elements can also improve isolation. By changing the orientation of one antenna, the relative polarizations of the antenna elements are changed accordingly, and this can offer better isolation [20]. A strip resonator embedded in-between the two radiators functions as a wave trap over the 2.4 and 5.2/5.8 GHz bands to enhance isolation between the two antennas by blocking the near-field radiating from one antenna to the other [21]. A metal strip was also employed to reduce mutual coupling [22, 23]. A feeding circuit having two T-shaped stubs, a parasitic-based microstrip line between the antennas, and a narrow slot on the ground plane were proposed in [24] to improve impedance matching and isolation. The decoupling approach based on a non-radiating circuit model was studied in [25]. An elliptical slot and a rectangular parasitic strip have been employed in [26].

Received 15 October 2021, Accepted 16 December 2021, Scheduled 27 December 2021

* Corresponding author: Khalil Hassan Sayidmarie (kh.sayidmarie@gmail.com).

[1] Institute of Technology, Northern Technical University, Mosul, Iraq. [2] College of Electronics Engineering, Ninevah University, Mosul, Iraq.

A multi-objective optimization method and fragment-type isolation structure were adopted in [27] to reduce the mutual coupling among antenna elements.

This work proposes a MIMO antenna system for WLAN applications. The proposed antenna covers the 2.45 GHz band (2.4 GHz–2.48 GHz), 5.25 GHz band (5.15 GHz–5.35 GHz), and 5.775 GHz band (5.725 GHz–5.825 GHz). The proposed structure consists of a MIMO antenna system with two dual-band monopoles placed close to each other with an edge-to-edge spacing of 7.3 mm ($0.0596\lambda_0$ at 2.45 GHz). The dual-band antenna element comprises a monopole of crescent shape to achieve a resonance frequency at the lower-band and an arc slot cut on the ground plane to achieve a resonance frequency at the upper band. Thus, the radiating element consists of two parts; a strip and a slot that is inspired by the self-complementary principle. The decoupling structure is based on two interlaced ring-shaped slots that are etched in the protruded ground plane in between the two monopoles. The ring-shaped slots within the decoupling structure disturb the surface current distribution on the ground plane such that the electromagnetic energy coupling between the ports is reduced, and hence good isolation is attained. This paper is organized as follows. Section 2 explains the proposed antenna structure, while in Section 3 the various design parameters are discussed, and their effects on the antenna performance are explored. The section also presents the experimental verification of the proposed design. A comparison of the achieved results of the proposed antenna with those of the published works is given in Section 4, and the drawn conclusions are listed in Section 5.

2. ANTENNA STRUCTURE

The geometry of the proposed dual-band MIMO antenna is shown in Fig. 1. The MIMO antenna consists of two crescent-shaped radiating elements of similar radii printed on a common grounded substrate. Each of the radiators is fed separately by a 50 Ω microstrip line, and the two arc slots are etched on the ground plane strip, which extends between the two radiating elements. An arc-shaped monopole and arc slot on the ground plane compose a dual-band antenna component, and the two antenna components are designed symmetrically. The antenna is designed on a 40 × 47.5 mm FR4 substrate with a dielectric constant of 4.3, a loss tangent of 0.025, and a thickness of 1.5 mm. The edge-to-edge distance (d) between the two arc slots is equal to 7.3 mm ($0.596\lambda_0$ at 2.45 GHz) where λ_o is the free-space wavelength. The dimensions of the proposed MIMO antenna are listed in Table 1.

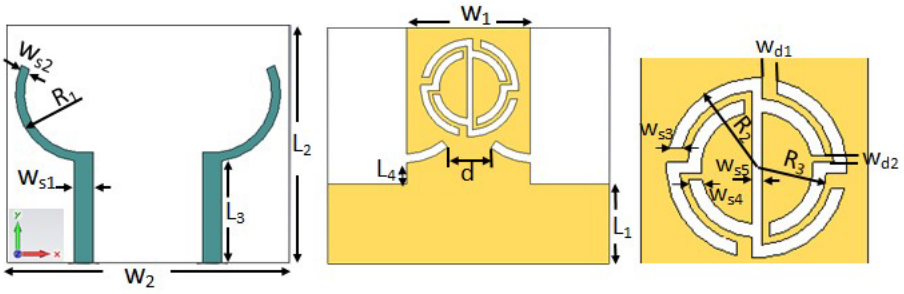

Figure 1. The structure of the proposed dual-band MIMO antenna, (a) front side, (b) back side, (c) enlarged view of the decoupling structure.

3. ANTENNA DESIGN

3.1. The Dual-Band Antenna Element

The composition of the element of the dual-band antenna is shown in Fig. 2(a). The antenna is made of a monopole of crescent-shaped strip and an arc-shaped slot etched on the ground plane that separate the two antennas. The average length of the monopole is set equal to about $\lambda_{e1}/4$ at the 2.45 GHz first band frequency, where λ_{e1} is the effective wavelength [28], while the average length of arc slot is equal to

Table 1. Parameters of the proposed MIMO antenna. All dimensions are in millimeters.

L_1	L_2	L_3	L_4	W_1	W_2	W_{s1}	W_{s2}
13.5	40	17	3.5	20.9	47.5	3.2	1.5
R_1	R_2	R_3	W_{S3}	W_{S4}	W_{S5}	Wd_1	Wd_2
11.5	8.3	6.4	1.2	1.25	1	1.36	0.63

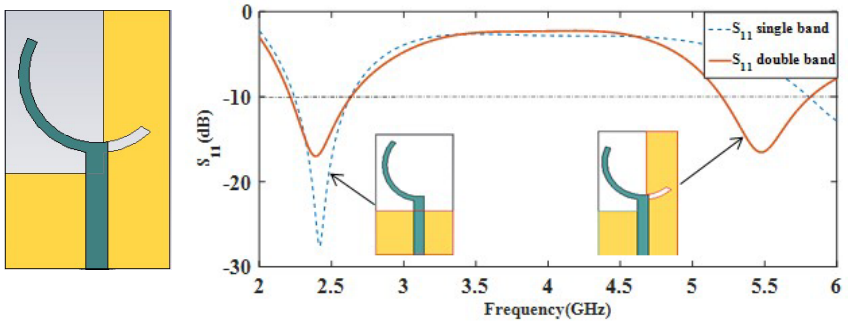

(a) (b)

Figure 2. (a) Geometry and (b) S_{11} of the dual-band antenna element.

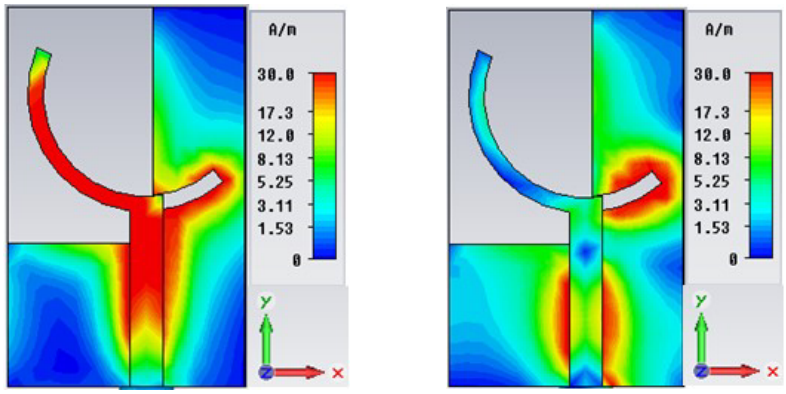

(a) (b)

Figure 3. Simulated surface current distributions at; (a) 2.45 GHz, and (b) 5.5 GHz.

$\lambda_{e2}/4$ at the 5.5 GHz at the resonance frequency of the second band. The simulated reflection coefficients S_{11} of the antenna element without and with the arc-shaped slot are shown in Fig. 2(b). As observed, the crescent-shaped monopole without the arc slot has an operating frequency at around 2.45 GHz with -10 dB impedance matching from 2.24–2.63 GHz. The arc-shaped slot on the ground plane provides an additional resonance frequency of 5.5 GHz with impedance matching from 5.16–5.855 GHz. Moreover, the current distributions at the three operating frequencies (2.45 GHz, 5.25 GHz, and 5.775 GHz) can be seen in Fig. 3. As shown, the main currents are on the crescent-shaped monopole at 2.45 GHz, while the stronger currents are distributed near the arc-shaped slot at a frequency of 5.5 GHz. Thus, we can conclude that the crescent-shaped monopole regulates the resonance of the lower-frequency band at 2.45 GHz, while the arc-shaped slot offers the impedance matching at the upper frequency bands (5.25 and 5.775 GHz). The obtained polar far-field radiation patterns for the proposed antenna are shown in Fig. 4 at the frequencies 2.45 GHz and 5.5 GHz. The shown patterns correspond to a typical monopole-like quasi-omnidirectional radiation pattern for the two principal planes. Moreover, the patterns at the

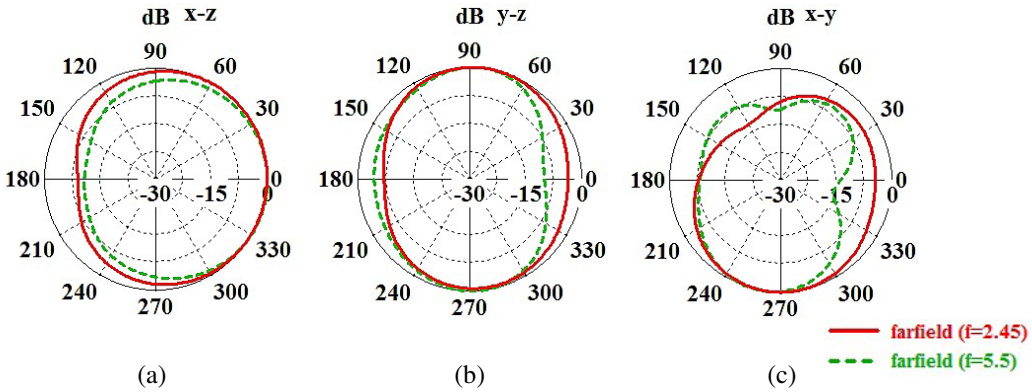

(a) (b) (c)

Figure 4. Simulated radiation patterns of the dual-band antenna element at the frequency of 2.45 GHz and 5.5 GHz for the; (a) x-z plane, (b) y-z plane, and (c) x-y plane.

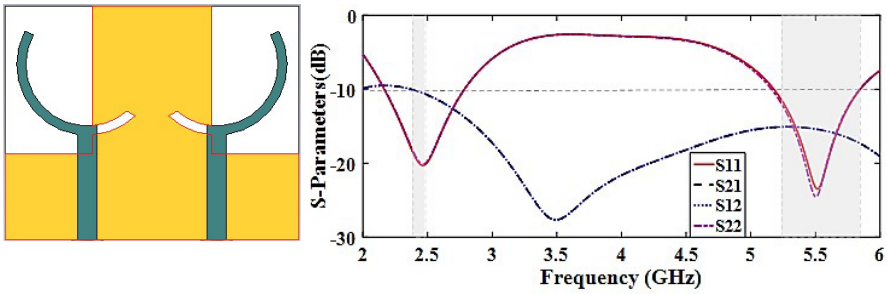

(a) (b)

Figure 5. (a) Geometry, (b) S-parameters of the MIMO antenna without the decoupling structure.

two bands are almost similar indicating stable patterns with frequency.

The simulated two-port S-parameters for the MIMO antenna without employing the decoupling element (reference antenna) are shown in Fig. 5(b). The results are obtained in the frequency range 2–6 GHz then analyzed for matching, bandwidth, and isolation performance. The simulated -10 dB impedance relative bandwidth is 25.3% at the first band with a center frequency of 2.45 GHz and 12.11% at the second band center frequency of 5.5 GHz. The mutual couplings are -10.47 dB and -15.37 dB at 2.45 GHz and 5.5 GHz across the two bands, respectively.

3.2. The Decoupling Structure

In order to reduce the mutual coupling at the two bands, two interlaced ring-shaped slots were etched in the ground plane strip between the two antennas. The proposed isolation technique is developed from the design of a wideband antenna element for the 5G communications [29]. The radius of the outer circle is fixed as 8.3 mm, while the radius of the inner circle is set as 6.4 mm as shown in Fig. 1 and Table 1. Slots with a length of $\lambda_e/2$ at the isolation frequencies are presented. The slot can be deliberated as a transmission line with short circuits at both ends. Thus it resonates when its length is equal to half the effective wavelength. For an isolation frequency (f_n), the length of such a slot is given by [30]:

$$l \cong \frac{\lambda_e}{2} \tag{1}$$

$$\lambda_e = \frac{c}{f_n \sqrt{\epsilon_e}} \tag{2}$$

$$\epsilon_e = \frac{(\epsilon_r + 1)}{2} + \frac{\epsilon_r - 1}{2}\left(\sqrt{1 + \frac{12h}{w}}\right)^{-1} \tag{3}$$

where l is the length of the slot, ε_e the effective dielectric constant, ε_r the relative permittivity of the substrate, and c the speed of the light. For the 2.45 GHz center frequency of the lower-band to be isolated, the total length of the slot line is evaluated to be 35 mm. Moreover, 15.56 mm is found for the 5.5 GHz operating frequency of the second band. The mean length of the bent structure (l_1) in Fig. 6(a) is equal to 19.58 mm and $l_1 = l_2$ due to the symmetry of the structure so that the total length of the two bent structures is equal to 39.16 mm. In Fig. 6(b) the average length of $l_3 = 7.94$ mm and the average length of $l_4 = 9.73$ mm, so that the total length of two arcs is equal to 17.67 mm. Fig. 6 shows the current distribution on the decoupling structure at the center frequency of the two bands. It is obvious that the signal passing through one of the coupling paths opposes the other signal from the other coupling path, so the mutual coupling can be reduced considerably.

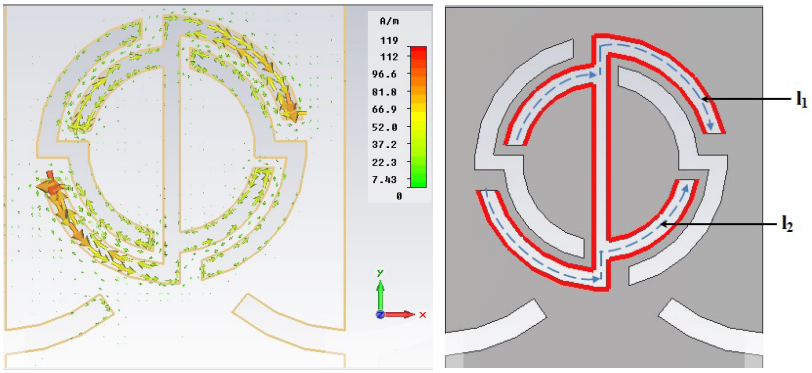

(a)

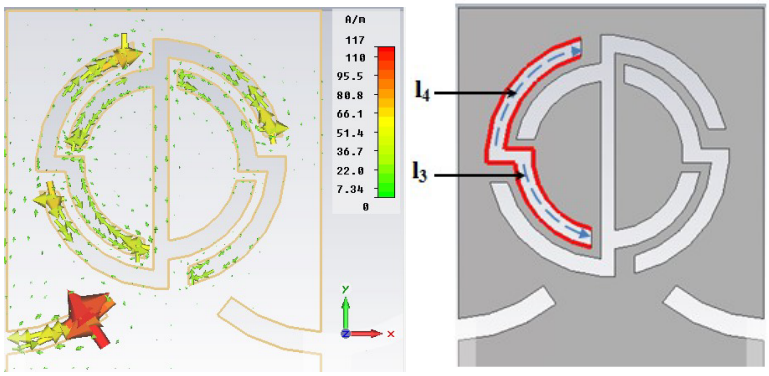

(b)

Figure 6. Current distributions when port-1 (left antenna element) is excited and the geometry of the decoupling structure, (a) at 2.45 GHz and (b) at 5.5 GHz.

3.3. The Parametric Study

Comprehensive parametric studies were conducted using the Time-Domain solver of CST in order to achieve the appropriate values of the two interlaced ring-shaped slots. A parametric study is implemented to explore the effect of the four parameters wd_1, wd_2, the position of a decoupling structure (y), and w_1. The obtained results are as shown in Figs. 7, 8, 9, and 10, respectively. In each case, one of the parameters is tuned, while the other parameters remain fixed as those in Table 1.

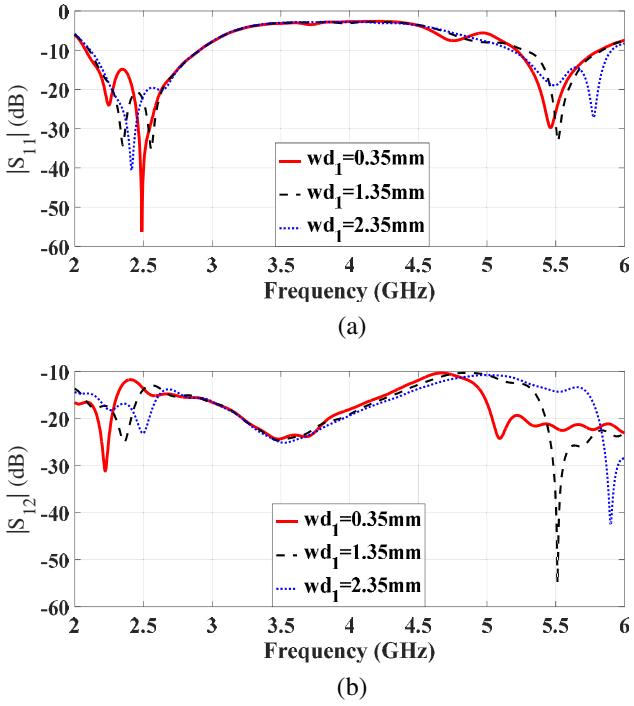

Figure 7. Simulation results of the (a) reflection coefficient S_{11}, and (b) coupling S_{12} against frequency for various values of wd_1.

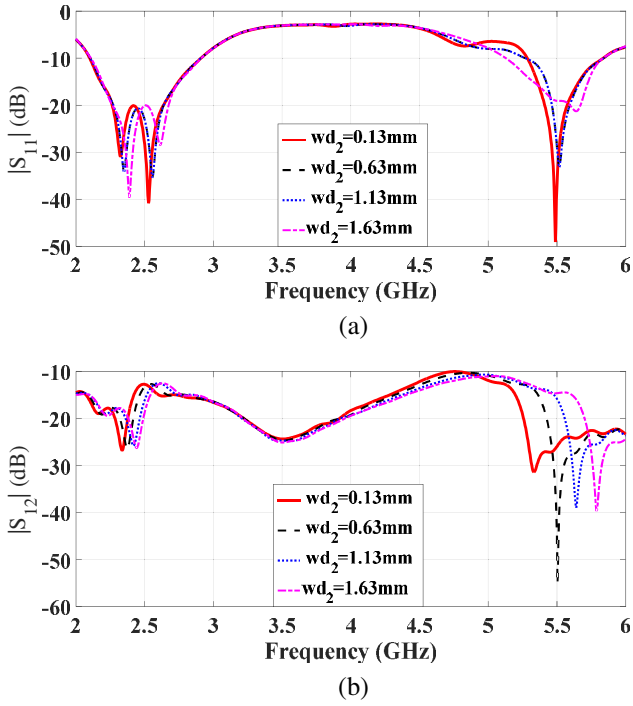

Figure 8. Simulation results of the (a) reflection coefficient S_{11}, and (b) coupling S_{12} against frequency for various values of wd_2.

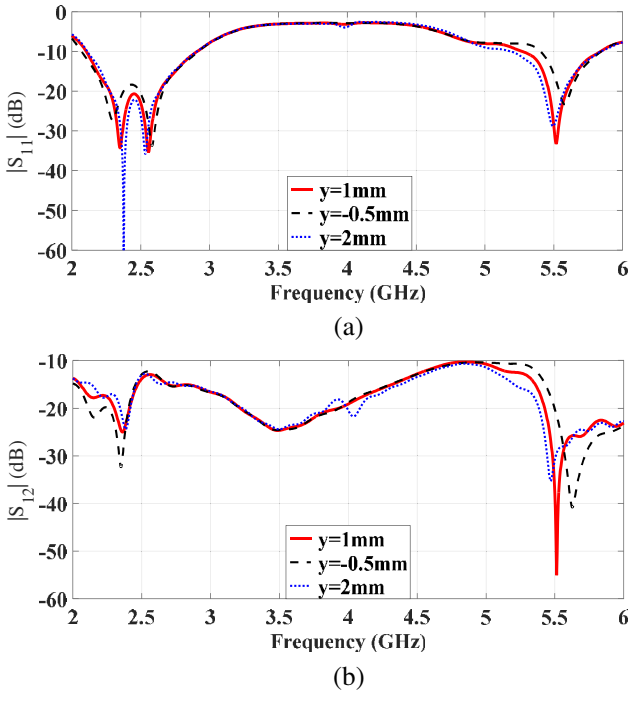

Figure 9. Simulation results of the (a) reflection coefficient S_{11}, and (b) coupling S_{12} against frequency for various values of y.

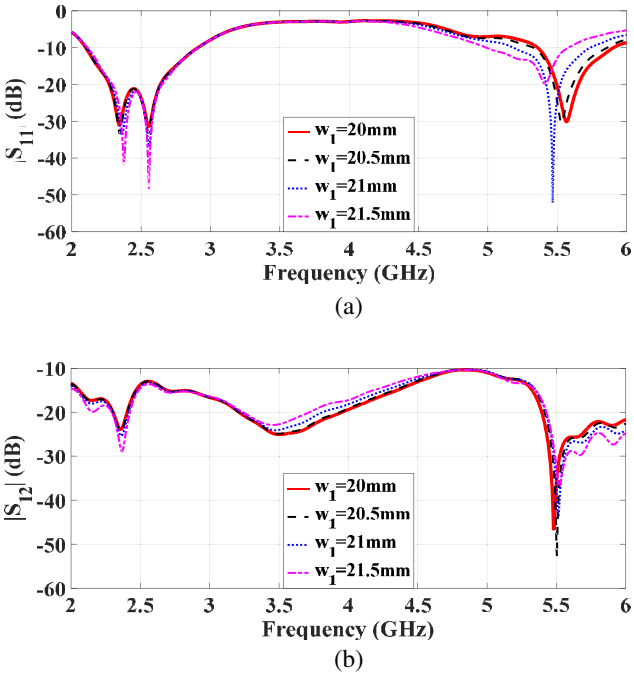

Figure 10. Simulation results of the (a) reflection coefficient S_{11}, and (b) coupling S_{12} against frequency for various values of w_1.

3.3.1. The Effect of wd_1

Figure 7 details the studies where wd_1 slot gap is presented with three different lengths (wd_1 = 0.35, 1.35, 235 mm). For increasing wd_1 the length of the bent slot on the decoupling structure reduces the frequencies of the lowest coupling (smaller S_{12}). It is noted that changing the slot length (wd_1) has a smaller effect on S_{11} performance.

3.3.2. The Effect of wd_2

Figure 8 details the studies when slot gap lengths wd_2 of (wd_2 = 0.13, 0.63, 1.13, 1.63 mm) are used. It can be observed that the slot length affects the bandwidth and mutual coupling of the proposed antenna. At the upper-band the bandwidth increased as wd_2 was increased. For S_{11} parameters, the frequency of maximum isolation was shifted to higher values for the two bands, and the mutual coupling S_{12} changed for the upper-band as wd_2 was increased.

3.3.3. The Effect of Position of the Decoupling Structure

Figure 9 shows the effect of the position of the decoupling structure on the ground plane for three different positions ($y = -0.5$, 1 and $y = 2$ mm) corresponding to the original position, which is located at $y = 0.5$ mm at Fig. 1 while keeping other parameters constant. The figure shows that the decoupling structure position influences the impedance bandwidth matching for the parameter of S_{11}. The matching is improved as the decoupling structure is moved up, and also the bandwidth of the second band increases as the decoupling structure is moved up. The decoupling position has also affected the coupling parameter S_{12}, and the isolation increases at the lower-frequency band as the position of the decoupling structure moves down in contrast with the higher frequency band where the isolation decreases when the decoupling structure moves down. At the upper-frequency band, the deep null of isolated frequency is shifted toward the higher frequency as the decoupling structure moves down.

3.3.4. The Effect of the Partial Ground Width (w_1)

Figure 10 shows the effect of the width of the partial ground plane for four different lengths (w_1 = 20, 20.5, 21, and 21.5 mm) while other parameters are kept constant. The change of the width of partial ground has influenced impedance matching and the value of mutual coupling especially on the upper band. As the width w_1 is increased, the average lengths of arc slots on the ground plane are increased which causes a decrease in the resonance frequency of the upper band. The matching and isolation are improved at the lower-band while, at the upper band, the frequency of maximum isolation changes as the w_1 is increased.

The above investigation has led to the following parameters that offer the best results (wd_1 = 1.36 mm, wd_2 = 0.63 mm, y = 0.5 mm, and w_1 = 20.9 mm).

3.4. Results and Discussions

The proposed antenna has been simulated, fabricated, and measured. In Fig. 11(b), the simulated S-parameters of the proposed antenna with the decoupling structure are presented. The mutual coupling between the antennas has been significantly reduced down to −19.32 dB and −55 dB at 2.45 and 5.5 GHz, respectively. A minimum mutual coupling of −55 dB is achieved at approximately 5.5 GHz, which represents a 39.68 dB improvement over the reference antenna (without the coupling structure). The measured and simulated S-parameters are in good agreement. The −10 dB bandwidth for the first band is 2.2–2.83 GHz, and that for the second band is 5.03–5.95 GHz. For the first band, the lowest measured isolation between the two ports is better than 20.6 dB, and for the second band, it is better than 17.85 dB. In terms of impedance bandwidth and isolation, the performance met the design criteria.

For further insight into the phenomenon of mutual coupling across the operating frequency bands of the proposed MIMO antenna, the simulated surface current distributions with and without the decoupling structure, when port-1 is excited and port 2 terminated with a 50 Ω load, are displayed in Fig. 12. Less current density is coupled from port-1 to port-2 in the antenna with the decoupling

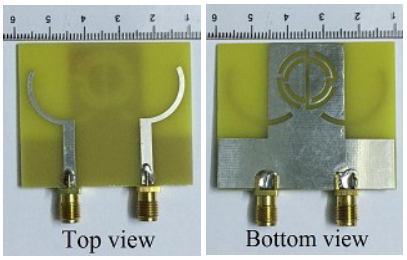

(a)

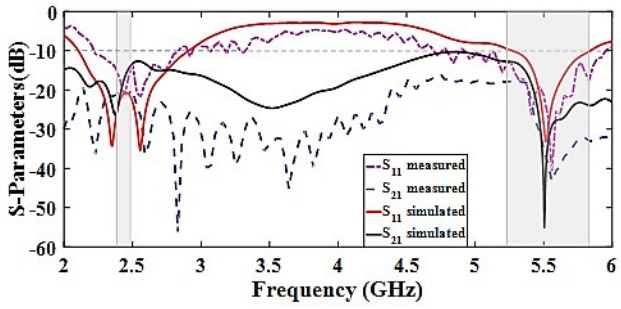

(b)

Figure 11. (a) The photograph of the prototype, (b) the measured and simulated S-parameters of the proposed MIMO antenna with the decoupling structure.

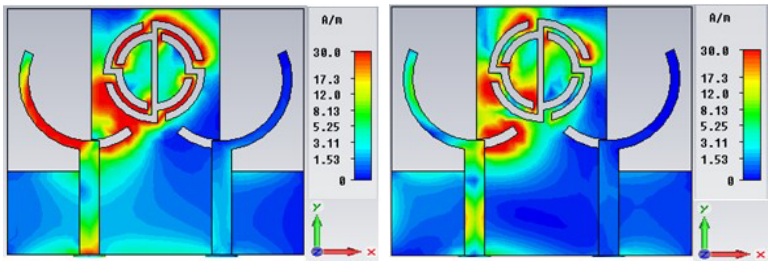

2.45 GHz 5.5 GHz

(a)

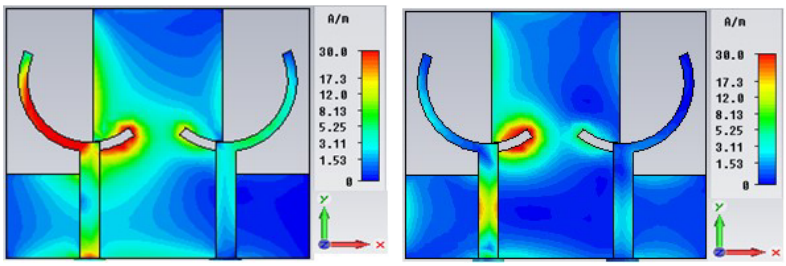

2.45 GHz 5.5 GHz

(b)

Figure 12. Current distributions at 2.45 GHz and 5.5 GHz when port-1 is excited and port-2 is terminated by a 50 Ω, (a) with and (b) without the decoupling structure.

structure than the antenna without the decoupling structure. The current is more intense around the two circular slots on the ground plane in the two frequency bands.

In Fig. 13, the simulated normalized radiation patterns at the two frequencies 2.45 and 5.5 GHz for the proposed (MIMO) antenna are plotted. The radiation patterns are drawn for the case where one of

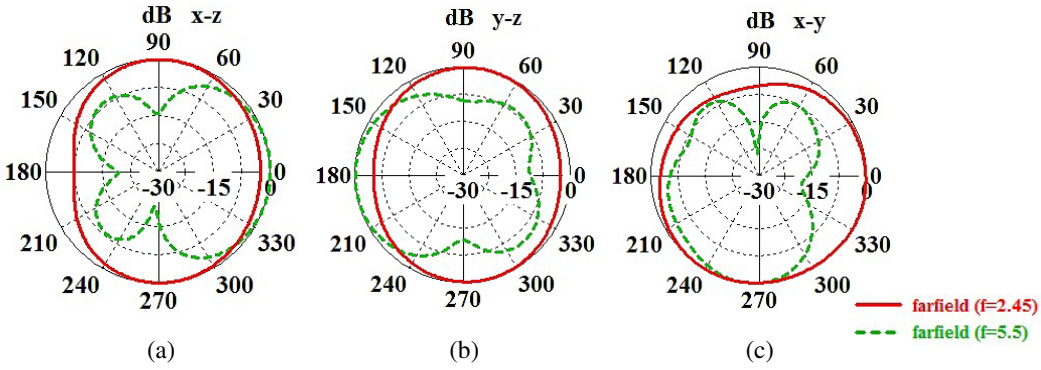

Figure 13. Simulated radiation patterns of MIMO antenna with decoupling structure at (a) x-z plane, (b) y-z plane, and (c) x-y plane.

the antennas is excited while the other is terminated with a matched load of 50 Ω. In comparison with the radiation patterns of the single element (shown in Fig. 4), the MIMO antenna preserves the same radiation pattern shape at the first band of 2.45 GHz. At the second band, some lobbing is seen, which can be attributed to the inclusion of the decoupling structure.

To asses the level of coupling between the two antennas and the influence of the decoupling structure in enhancing the isolation, the envelope correlation coefficient (ECC) of the proposed MIMO antenna is evaluated. This coefficient can be calculated from the 3-D far-field radiation pattern using the following formula [26]:

$$ECC = \frac{\left|\iint_{4\pi}^{0}\left[\overrightarrow{F_1}(\theta,\Phi)\cdot\overrightarrow{F_2}(\theta,\Phi)\right]d\Omega\right|^2}{\left|\iint_{4\pi}^{0}\left[\overrightarrow{F_1}(\theta,\Phi)\right]d\Omega\right|^2\left|\iint_{4\pi}^{0}\left[\overrightarrow{F_2}(\theta,\Phi)\right]d\Omega\right|^2} \tag{4}$$

where the mark $(\cdot)$ represents the Hermitian product; dΩ represents the differential solid unit angle; $F(\ )$ denotes the antenna's field radiation pattern obtained by exciting one port while the other port is terminated by a load of 50 ohms. For the MIMO antenna analyzed in this study, the obtained envelope correlation coefficients against frequency are shown in Fig. 14, where a maximum value of 0.017 for the first band and 0.004 for the second band are evident. The introduction of the two interlaced ring-shaped slots has considerably reduced the values of the ECC at the lower-band, and improvement is seen at the upper-band. In addition, it can be seen that the desired ECC demands good performances in impedance matching and isolation.

The simulated gain and total radiation efficiency at the WLAN bands are shown in Fig. 15. The gain is equal to 1.99 dB with the corresponding efficiency of 88.5% at 2.45 GHz, while the gain is equal to 4.71 dB with the corresponding efficiency of 75.82% at 5.5 GHz. Higher gain is usually achieved at

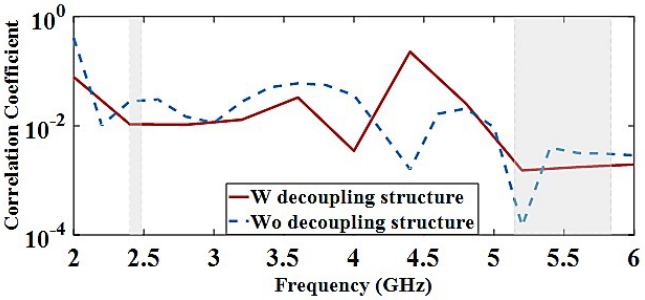

Figure 14. Envelope correlation coefficients of the proposed MIMO antenna with and without the decoupling structure.

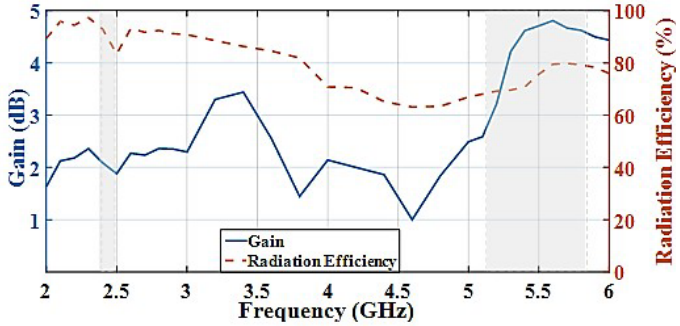

Figure 15. Gain and total radiation efficiency when port 1 is excited and port 2 is matched-loaded.

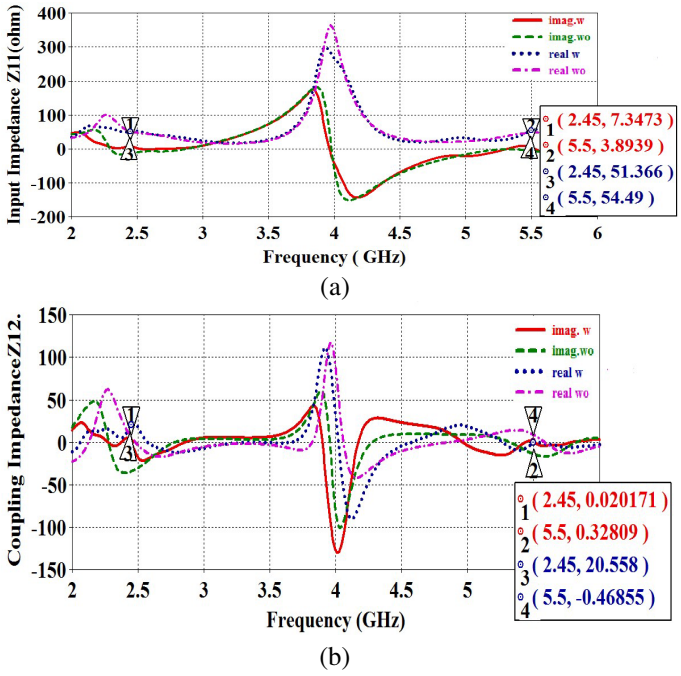

Figure 16. The Z-parameters of the proposed antenna; (a) the input impedance Z_{11}, (b) the mutual impedance Z_{12}.

higher frequency, while the efficiency is slightly smaller at the upper band due to the higher loss of the substrate.

Figure 16 displays the Z-parameters of the proposed antenna. Fig. 16(a) depicts the antenna self impedance Z_{11} before and after introducing the decoupling structure. According to the figure, two anti-resonance modes are matched to about 50 Ω in the investigation band (2 GHz–6 GHz). At 2.45 GHz. The first resonance corresponds to the 51 Ω impedance, while at 5.5 GHz, the second resonance corresponds to the 54 Ω. The proposed antenna's coupling impedance Z_{12} is shown in Fig. 16(b). At 2.45 GHz the mutual impedance decreases from 20.558 Ω to 0.02 Ω with the introduction of the decoupling structure. The improvement at 5.5 GHz is from 0.468 Ω to 0.328 Ω. Thus, the addition of the decoupling structure has reduced the mutual impedance towards zero leading to much lower mutual coupling.

4. COMPARISON WITH PUBLISHED WORKS

The performances of prevailing MIMO antennas with different techniques in terms of important performance metrics such as frequency range, antenna size separation distance, and isolation

improvement at the operating frequency are compared with the proposed antenna as shown in Table 2. The proposed antenna is smaller than those reported in [5, 6, 10, 18, 19, 27, 31]. In [2, 5, 10, 24, 27], the authors have studied the isolation for a single band only. In [5, 6, 18, 22, 26, 27, 31], the claimed tiny distance for the edge-to-edge distance between the antennas is relatively larger than that in the proposed work. The results in Table 2 show a reasonably superior isolation performance at the second frequency band as compared with all other reported designs.

Table 2. Performance comparison of the proposed antenna with previously published work found in the literature.

Ref. No.	Resonance freq. or freq. range in (GHz)	Overall antenna dimensions & volume (mm)	Edge to edge distance	Isolation improvement in (dB)	ECC	Gain (dB)	Efficiency (%)
2	5.7–6.3	$46 * 20 * 1.6 = 1472$	$0.15\lambda_0 = 7.86$ mm	21.8	0.01	N.A	N.A
5	5	$78 * 60 * 1.6 = 7488$	$0.2\lambda_0 = 12$ mm	31	N.A	4.04	51.51
6	2.1–3.03 3.45–4.97 7.15–7.94	$90 * 50 * 0.8 = 3600$	$0.256\lambda_0 = 30$ mm	$\cong 10$ $\cong 3$ -	0.025 0.02 0.0025	1.3 3.5 1	N.A
10	1.43–3.7	$70 * 120 * 1.5 = 12768$	$0.06\lambda_0 = 8$ mm	> 15	0.03	2.14	N.A
18	2.4, 5.2	$40 * 80 * 1 = 3200$	12.5 mm	10 $\cong 8$	< 0.05	3.5 4.57	N.A
19	2.46–2.7 5.04–5.5	$47.3 * 74 * 1.6 = 5600$	$0.044\lambda_0 = 5.3$ mm	25 3	< 0.01	2.59, 3	93.3, 85.9
22	2.35–2.65 4.9–6.2	$26 * 50 * 0.8 = 1040$	17.6 mm	5.4	< 0.06	1.56, 4.43	70.1, 82.3
24	5.33–5.62	$40 * 32 * 1 = 1280$	$0.018\lambda_0 = 1$ mm	37.7	< 0.15	4.79	73
26	3.2–3.8 5.7–6.2	$30 * 26 * 1.6 = 1248$	$0.1167\lambda_0 = 10$ mm	20 20	< 0.03 < 0.03	1.5 2.8	N.A
27	3.42–3.5	$86 * 43 * 1.6 = 5916$	$0.144\lambda_0 = 12$ mm	8	N.A	N.A	N.A
31	2.2–2.5 3.3–3.8 5.4–7.17	$40 * 75 * 1.6 = 4800$	$0.08\lambda_0 = 10$ mm	$\cong 22$	N.A	N.A	N.A
This work	2.1–2.9 5.13–5.845	$40 * 47.5 * 1.5 = 2850$	$0.0596\lambda_0 = 7.3$ mm	8.85 39.63	< 0.017 < 0.004	1.99 4.71	88.5 75.82

5. CONCLUSION

In this paper, a double-band MIMO antenna system with high isolation is suggested. The high isolation is attained by cutting two interlaced ring-shaped slots on the ground plane that protrudes between the two antennas. The two antenna elements are spaced by a small distance of only $0.0596\lambda_0$ at 2.45 GHz. The simulated results indicate that the operating frequency can cover 2.45, 5.2, and 5.775 GHz WLAN bands with maximum isolation of 19.3 dB at 2.45 GHz and 55 dB at 5.5 GHz. The gain is equal to 1.99 dB with the corresponding efficiency of 88.5% at the first band, while the gain is equal to 4.71 dB with the corresponding efficiency of 75.82% at the second band. The measured isolation is more than 17.85 dB in all covered bands. Furthermore, the proposed MIMO antenna system has extremely small envelop correlation coefficients. The design is suitable for MIMO technology.

REFERENCES

1. Luo, C.-M., J.-S. Hong, and L.-L. Zhong, "Isolation enhancement of a very compact UWB-MIMO slot antenna with two defected ground structures," *IEEE Antennas and Wireless Propagation Letters*, Vol. 14, 1766–1769, 2015, DOI:10.1109/LAWP.2015.2423318.
2. Kumar, N. and U. K. Kommuri, "MIMO antenna H-plane isolation enhancement using UC-EBG structure and metal line strip for WLAN applications," *Radio Engineering*, Vol. 28, No. 2, 399–406, Jun. 2019.
3. Isaac, A. A., H. M. Al-Rizzo, A. I. Hammoodi, S. Abushamleh, and H. R. Khaleel, "Isolation enhancement of two planar monopole antennas for MIMO wireless applications," *2015 IEEE International Symposium on Antennas and Propagation & USNC/URSI National Radio Science Meeting*, 380–381, 2015, DOI: 10.1109/APS.2015.7304576.
4. Ghosh, J., S. Ghosal, D. Mitra1, and S. R. B. Chaudhuri, "Mutual coupling reduction between closely placed microstrip patch antenna using meander line resonator," *Progress In Electromagnetics Research Letters*, Vol. 59, 115–122, 2016.
5. Li, Q., C. Ding, R. Yang, M. Tan, G. Wu, X. Lei, X. Jiang, S. Fang, M. Huang, Y. Gong, and Y. Wei, "Mutual coupling reduction between patch antennas using meander line," *International Journal of Antennas and Propagation*, 1–7, Article ID 2586382, 2018.
6. Kumar, A., A. Q. Ansari, B. K. Kanaujia, J. Kishor, and P. Kandpal, "Design of CPW-Fed triple-band two-port MIMO antenna with U shaped slot isolation structure for high isolation," *2018 IEEE MTT-S International Microwave and RF Conference (IMaRC)*, 1–4, Kolkata, India, Nov. 28–30, 2018, DOI: 10.1109/IMaRC.2018.8877330.
7. Yahya, L. S., K. H. Sayidmarie, F. Elmegri, and R. A. Abd-Alhameed, "Crescent-shaped double-monopole antennas with reduced coupling for WLAN and WIMAX applications," *2015 Internet Technologies and Applications (ITA)*, 393–398, Wales, UK, Sept. 8–11, 2015.
8. Yahya, L. S., K. H. Sayidmarie, F. Elmegri, and R. Abd-Alhameed, "Arc-shaped monopole antennas with reduced coupling for WLAN and WIMAX applications," *2017 Internet Technologies and Applications (ITA)*, 218–223, Wrexham, UK, Sep. 12–15, 2017, DOI: 10.1109/ITechA2017.8101942.
9. Ikram, M., N. N.-Trong, and A. Abbosh, "Multiband MIMO microwave and millimeter antenna system employing dual-function tapered slot structure," *IEEE Transactions on Antennas and Propagation*, Vol. 67, No. 8, 5705–5710, 2019, DOI 10.1109/TAP.2019.2922547.
10. Isaac, A. A., H. Al-Rizzo, S. Yahya, and S. Abushamleh, "Decoupling of two closely-spaced planar monopole antennas using two novel printed-circuit structures," *Microwave and Optical Technology Letters*, Vol. 60, 2954–2963, 2018, https://doi.org/10.1002/mop.31405.
11. Aruna, S., H. Ismat, and K. S. Naik, "A very small dual-band MIMO slot antenna for WLAN and WiMAX applications," *IOSR Journal of Electronics and Communication Engineering (IOSR-JECE)*, Vol. 13, No. 6, Ver. I, 39–45, 2018.
12. Bhanumathi, V. and G. Sivaranjani, "High isolation MIMO antenna using semi-circle patch for UWB applications," *Progress In Electromagnetics Research C*, Vol. 92, 31–40, 2019.
13. Sui, J., Y. Dou, X. Mei, and K.-L. Wu, "Self-curing decoupling technique for MIMO antenna arrays in mobile terminals," *IEEE Transactions on Antennas and Propagation*, Vol. 68, No. 2, 838–849, Feb. 2020.
14. Diallo, A., C. Luxey, P. L. Thuc, R. Staraj, and G. Kossiavas, "Reduction of the mutual coupling between two planar inverted-F antennas working in close frequency bands," *Automatika*, Vol. 47, Nos. 3–4, 113–120, 2006.
15. Chen, Y.-S. and H.-C. Zhou, "An isolation-enhanced quad-element antenna using suspended solid wires for LTE small-cell base stations," *Radio Science*, Vol. 52, No. 5, 663–676, 2017.
16. Huang, J.-H., W.-J. Chang, and C. F. Jou, "Dual-band MIMO antenna with high isolation application by using neutralizing line," *Progress In Electromagnetics Research Letters*, Vol. 48, 15–19, 2014.
17. Khade, S. S. and S. L. Badjate, "A compact multiband U shape MIMO antenna for wireless application," *International Journal of Wireless and Microwave Technologies*, Vol. 6, 61–71, 2016,

DOI: 10.5815/ijwmt.2016.05.07.

18. Kim, J., M. Han, C. Lee, and J. Choi, "Dual band MIMO antenna using a decoupling network for WLAN application," *13th International Conference on Advanced Communication Technology (ICACT2011)*, 624–627, Feb. 13–16, 2011.
19. Liu, P., D. Sun, P. Wang, and P. Gao, "Design of a dual-band MIMO antenna with high isolation for WLAN applications," *Progress In Electromagnetics Research Letters*, Vol. 74, 23–30, 2018.
20. Mohammad, S., A. Nezhad, H. R. Hassani, and A. Foudazi, "A dual-band WLAN/UWB printed wide slot antenna for MIMO/diversity applications," *Microwave and Optical Technology Letters*, Vol. 55, No. 3, 461–465, Mar. 2013, DOI 10.1002/mop.
21. Kang, T.-W. and K.-L. Wong, "Isolation improvement of 2.4/5.2/5.8 GHz WLAN internal laptop computer antennas using dual-band strip resonator as a wave trap," *Microwave and Technology Letters*, Vol. 52, No. 1, 58–64, Jan. 2010, DOI 10.1002/mop.
22. Luo, C.-M., J.-S. Hong, and M. Amin, "Mutual coupling reduction for dual-band MIMO antenna with simple structure," *Radio Engineering*, Vol. 26, No. 1, 51–56, DOI: 10.13164/re.2017.0051.
23. Bhaskar, P. V., V. Krishnanaik, and M. Naganaik, "A tapered fed MIMO antenna for IEEE INSAT band using L-slits," *International Journal of Engineering and Techniques*, Vol. 4, No. 2, 980–988, ISSN: 2395-1303, Mar.–Apr. 2018.
24. Ghannad, A. A., M. Khalily, P. Xiao, R. Tafazolli, and A. A. Kishk, "Enhanced matching and vialess decoupling of nearby patch antennas for MIMO system," *IEEE Antennas and Wireless Propagation Letters*, Vol. 18, No. 6, 1066–1070, Jun. 2019.
25. Cheng, P., D. Sun, P. Wang, and P. Gao, "A dual-band MIMO antenna using a passive circuit for isolation enhancement," *Progress In Electromagnetics Research Letters*, Vol. 71, 117–123, 2017.
26. Nirmal, P. C., A. Nandgaonkar, S. Nalbalwar, and R. K. Gupta, "A compact dual-band MIMO antenna with improved isolation for WI-MAX and WLAN applications," *Progress In Electromagnetics Research M*, Vol. 68, 69–77, 2018.
27. Ding, D., D. Li, T. Tang, D. Min, and Q. Zhang, "A $2*2$ MIMO antenna design with high isolation, and steady radiation performances," *IOP Conf. Series: Materials Science and Engineering*, Vol. 768, 062081, 1–6, 2020, doi:10.1088/1757-899X/768/6/062081.
28. Sayidmarie, K. H. and L. S. Yahya, "Design and analysis of dual-band crescent-shape monopole antenna for WLAN applications," *International Journal of Electromagnetic and Applications*, Vol. 3, No. 4, 96–102, 2013.
29. Wang, F., Z. Duan, X. Wang, Q. Zhou, and Y. Gong, "High isolation millimeter-wave wideband MIMO antenna for 5G communication," *International Journal of Antennas and Propagation*, Vol. 2019, 1–12, Article ID4283010, 2019, doi.org/10.1155/2019/4283010.
30. Kumer, G. and K. P. Ray, *Broadband Microstrip Antennas*, Artech House, 2003.
31. Iddi, H. U., R. Kamarudin, T. A. Rahman, A. Y. Abdurahman, R. Dewan, and A. S. Azini, "Triple band planar monopole antenna for MIMO application," *PIERS Proceedings*, 1421–1424, Stockholm, Sweden, Aug. 12–15, 2013.